Computational and Structural Biotechnology Journal 17 (2019) 797–804

COMPUTATIONAL AND STRUCTURAL BIOTECHNOLOGY JOURNAL

journal homepage: www.elsevier.com/locate/csbj

Mini Review

Base-pair Opening Dynamics of Nucleic Acids in Relation to Their Biological Function☆

Seo-Ree Choi [a], Na-Hyun Kim [a], Ho-Seong Jin [a], Yeo-Jin Seo [a], Juhyun Lee [b], Joon-Hwa Lee [a,*]

[a] Department of Chemistry and RINS, Gyeongsang National University, Gyeongnam 52828, South Korea
[b] Department of Chemistry, KAIST, Daejeon 34141, South Korea

ARTICLE INFO

Article history:
Received 28 February 2019
Received in revised form 20 May 2019
Available online 13 June 2019

Keywords:
NMR
Nucleic acids
Base-pair opening
Hydrogen exchange
DNA
RNA

ABSTRACT

Base-pair opening is a conformational transition that is required for proper biological function of nucleic acids. Hydrogen exchange, observed by NMR spectroscopic experiments, is a widely used method to study the thermodynamics and kinetics of base-pair opening in nucleic acids. The hydrogen exchange data of imino protons are analyzed based on a two-state (open/closed) model for the base-pair, where hydrogen exchange only occurs from the open state. In this review, we discuss examples of how hydrogen exchange data provide insight into several interesting biological processes involving functional interactions of nucleic acids: *i*) selective recognition of DNA by proteins; *ii*) regulation of RNA cleavage by site-specific mutations; *iii*) intermolecular interaction of proteins with their target DNA or RNA; *iv*) formation of PNA:DNA hybrid duplexes.

Contents

1. Introduction

Base-pair opening in DNA is a structural fluctuation that is required for its biological function in transcription, repair, and

☆ This work was dedicated to Professor Byong-Seok Choi on the occasion of his retirement and 65th birthday.

* Corresponding author.
E-mail address: joonhwa@gnu.ac.kr (J.-H. Lee).

https://doi.org/10.1016/j.csbj.2019.06.008

recombination. RNA also undergoes conformational transitions that exhibit distinct structural and dynamic features required for proper function. The hydrogen-bonded imino protons of nucleic acids are a probe of the base-pair opening kinetics. Hydrogen exchange NMR experiments provide information on the thermodynamics and kinetics of base-pair opening and therefore represent a probe of the dynamic motions of the base-pairs. Analysis of the hydrogen exchange of imino protons employs a two-state (open/closed) model for the base-pair, where hydrogen exchange only occurs from the open state (Fig. 1) [1–3]. The opening (k_{op}) and closing (k_{cl}) rate constants and/or equilibrium constant for base-pair opening ($K_{op} = k_{op}/k_{cl}$) can be determined by measuring the exchange using an external catalyst. These experiments have been used to probe base-pair opening in various DNA duplexes [3–18], DNAs containing modified base such as 5-flurourasil, N6-methyl adenine, or modified guanine [19–21], UV-induced photoadduct-containing DNA [22], IHF-complexed DNA [23], interstrand cross-linked DNA [24], i-motif structure formed by the complementary C-rich DNA [25,26], various RNAs [15,27–36], peptide nucleic acids (PNAs) [37,38], and threose nucleic acid (TNA) [39]. NMR exchange and single molecule FRET experiments could be used to study the protonation/deprotonation of adenine bases and formation of $A^+ \cdot C$ wobble pair [40–44]. In addition, hydrogen exchange data can also be used to probe how intermolecular interactions stabilize nucleic acid duplexes. For example, imino proton exchange studies of a DNA/RNA-protein complex by NMR spectroscopy showed that the protein substantially changes the equilibrium constant for base-pair opening [45–49].

In this review, we discuss several examples of how hydrogen exchange data provide insight into the biological function of interesting nucleic acids. Studies of base-pair opening kinetics have been used to propose mechanisms by which DNA is selectively recognized by its target proteins. Selective recognition is used by seqA to distinguish the hemimethylated GATC from the corresponding fully methylated complex [20], and the higher binding affinity of XPC-hHR23B for a double mismatched cyclobutane pyrimidine dimer (CPD) helps it distinguish the double mismatch from the matched or single mismatched CPD species [22]. Base-pair opening kinetics studies can also suggest the mechanisms that explain how RNA cleavage can be regulated by site-specific mutations, e.g., in the case of the biogenesis of miRNA156a by DICER-like 1 protein (DCL1) [31] and self-cleavage of the *Tetrahymena* group I ribozyme [28]. Hydrogen exchange studies can elucidate the intermolecular interactions of proteins with their target DNA or RNA, as in the case of B-Z transition of DNA [50] and B-Z junction formation [49] facilitated by *Z*-DNA binding proteins (ZBPs), and VEGF-targeting of RNA aptamers [51]. Finally, we also describe recent hydrogen exchange studies of a PNA:DNA hybrid duplex [38].

2. Hydrogen Exchange Theory

2.1. Hydrogen Exchange of the Base-Paired Imino Protons

Imino proton exchange from a base-pair consists of a two-step process requiring base-pair opening followed by proton transfer to a base catalyst (Fig. 1). The rate constant for imino proton exchange (k_{ex}) is given by Eq. (1):

$$k_{ex} = \frac{k_{op} \times k_{tr}}{k_{cl} + k_{tr}} \tag{1}$$

where k_{op} and k_{cl} are the rate constants for opening and closing of the base-pair, respectively, and k_{tr} is the rate constant for proton exchange by base catalyst in the opening state. In the base-pair, the exchange is

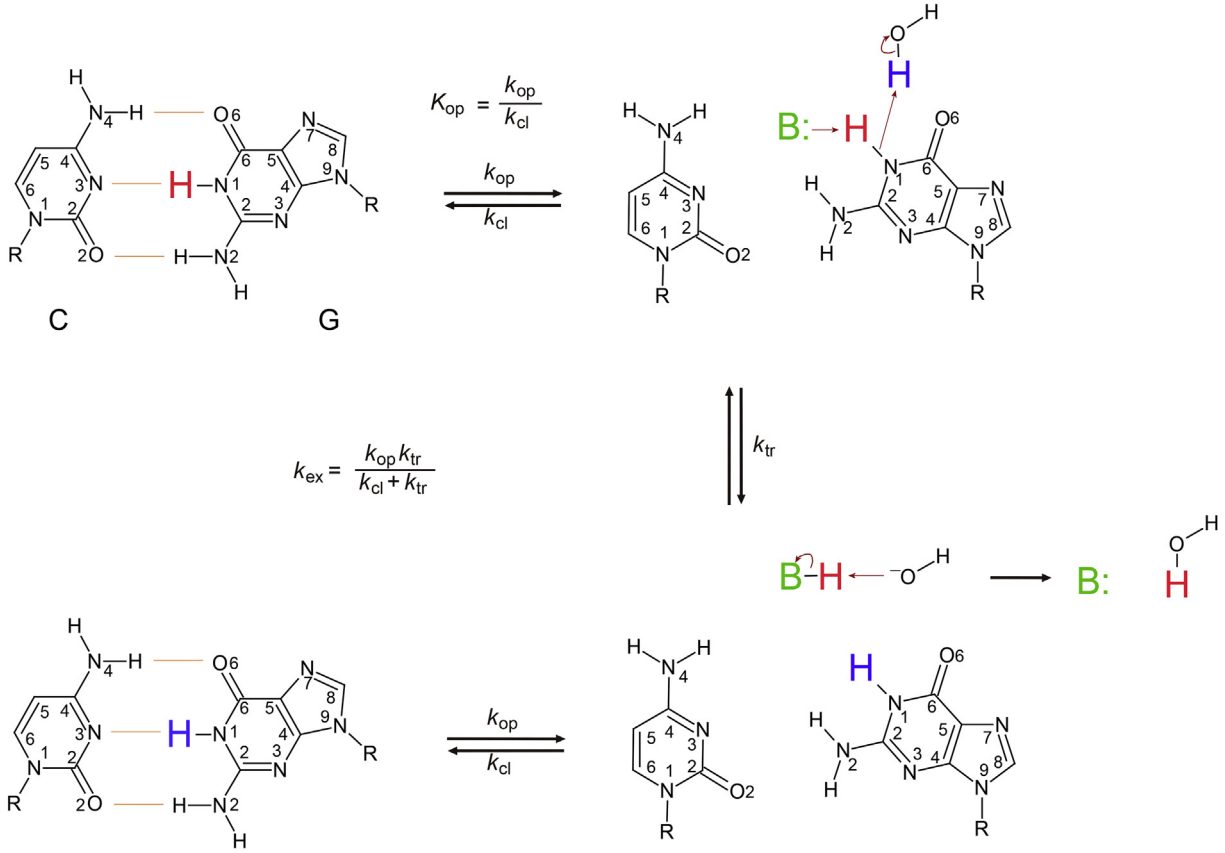

Fig. 1. Two-state (open/closed) model for the base-pair, where hydrogen exchange of the imino proton only occurs from the open state by the base catalyst (B:).

catalyzed by both the added base catalyst and the nitrogen of the complementary base, which acts as an intrinsic catalyst [1,2]. The k_{tr} value is calculated as:

$$k_{tr} = k_B[B] + k_{int} = \frac{k_{coll}}{1 + 10^{\Delta pK_a}}[B] + k_{int} \quad (2)$$

where k_B is the rate constant for imino proton transfer by a base catalyst, k_{int} is the exchange rate constant catalyzed by an intrinsic base, k_{coll} is the collision rate constant, [B] is the concentration of the externally added base catalyst such as ammonia, Tris, phosphate, and difluoroethylamine (base form) and ΔpK_a is the pK_a difference between the imino proton and the base catalyst. The [B] values are calculated as $[B] = [B]_{total}/(1 + 10^{(pKa-pH)})$, where $[B]_{total}$ is the total concentration of the added base catalyst [28,38]. Thus, the k_{ex} for the base-paired imino proton is represented by Eq. (3):

$$k_{ex} = \frac{k_{op}(k_B[B] + k_{int})}{k_{cl} + (k_B[B] + k_{int})} = \frac{k_{op}(k_B[B] + k_{int})}{k_B[B] + k_{int} + k_{op}/K_{op}} \quad (3)$$

where K_{op} ($= k_{op}/k_{cl}$) is the equilibrium constant for base-pair opening. *Re*-organization of Eq. (3) yields the following equation:

$$\tau_{ex} = \frac{1}{k_{ex}} = \frac{1}{k_{op}} + \frac{1}{K_{op}}\frac{1}{k_B[B] + k_{int}} = \tau_0 + \frac{1}{K_{op}(k_B[B] + k_{int})} \quad (4)$$

where τ_{ex} is the exchange time ($= 1/k_{ex}$) and τ_0 is the lifetime for closed state of the base-pair ($= 1/k_{op}$). Interestingly, curve fitting the τ_{ex} of the imino protons as a function of the concentration (base form) of the added base catalyst ([B]) within Eq. (4) gives not only the thermodynamic parameter, K_{op}, but also kinetic parameter, τ_0 ($= 1/k_{op}$) value (Fig. 2A) [31,32]. As [B] increases, the τ_{ex} values converge to the base-pair lifetime, τ_0, in these plots. For example, the U16·A97 base-pair in the wild-type (WT) primary miRNA156a model RNA is expected to have a longer τ_0 than that of the A9C and A10CG mutants (τ_0 of WT, 5.0 ms; A9C, 1.0 ms; A10CG, 1.6 ms) (Fig. 2A) [31]. The lifetime for open state of the base-pair ($\tau_{open} = 1/k_{cl}$) is calculated using the relation $\tau_{open} = K_{op} \times \tau_0$.

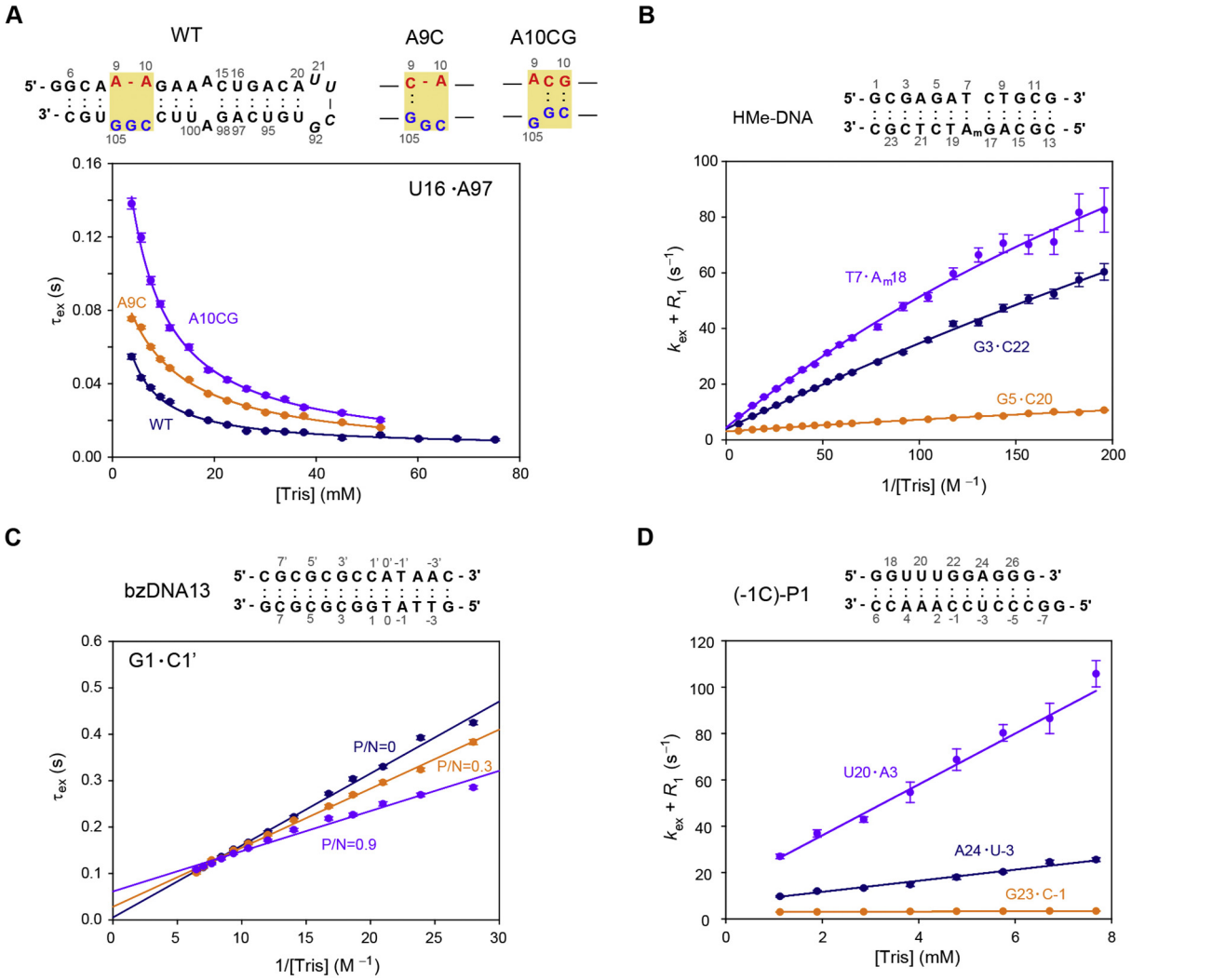

Fig. 2. Hydrogen exchange data of the (A) primary miRNA156a modeled RNA (pri-miR156a) [33], (B) DNA dodecamer duplex containing hemimethylated GATC site (HMe-GATC) [20], (C) DNA 13mer duplex (bzDNA13) complexed with $Z\alpha_{ADAR1}$ [39], and (D) (-1C)-mutant P1 RNA duplex ((-1C)-P1) [30]. The solid lines are the best fits to Eqs. (4), (5), (6), and (7), respectively, and the error bars represent the fitting errors during determination of R_{1a} ($= R_1 + k_{ex}$) or τ_{ex} ($= 1/k_{ex}$) values. [Tris] is the concentration of Tris (base form) which is used for the base catalyst. Secondary structures of the wild-type (WT) and A9C and A10CG mutant pri-miR156a (in (A)), HMe-GATC (in (B)), bzDNA13 (in (C)), and (-1C)-P1 (in (D)) are shown on top of each hydrogen exchange data.

Under certain conditions where $k_B[B]$ is much larger than k_{int}, Eq. (3) simplifies to Eq. (5):

$$k_{ex} = \frac{k_{op}k_B[B]}{k_B[B] + k_{op}/K_{op}} = \frac{k_B k_{op}[B]}{k_B[B] + k_{cl}} \quad (5)$$

In this case, parameters for the base-pair opening dynamics can be determined by curve fitting the exchange data using Eq. (5) (Fig. 2B) [20,21]. The apparent relaxation rate constant (R_{1a}) for an imino proton determined by NMR experiments is the sum of the k_{ex} value and the R_1 relaxation rate constant. As [B] increased, the k_{ex} values converge to the k_{op} value in these plots. For example, in duplex DNA containing a hemimethylated GATC site, the T7·A18 and G3·C22 base-pairs are expected to have larger k_{op} (that is, shorter τ_0) than the G5·C20 base-pair (τ_0 of T7·A18, 2.4 ms; G3·C22, 2.0 ms; G5·C20, 24.4 ms) (Fig. 2B) [20]. Similarly, under these conditions ($k_B[B] >> k_{int}$), Eq. (4) becomes:

$$\tau_{ex} = \tau_0 + \frac{1}{k_B K_{op}[B]} \quad (6)$$

Curve fitting the τ_{ex} as a function of the inverse of [B] (1/[B]) with Eq. (6) gives the K_{op} and τ_0 values (Fig. 2C) [38,49]. The slope of the linear correlation between τ_{ex} and 1/[B] is τ_0 and the y-intercept is $1/(k_B K_{op})$. Thus, the imino proton of a more slowly opened base-pair with longer τ_0 has a larger y-intercept, while that of a less stable base-pair with larger K_{op} has a smaller slope in these plots. For example, in the DNA duplexes complexed with the Zα domain of human double-stranded RNA deaminase I, ADAR1, ($Z\alpha_{ADAR1}$), the G1·C1′ base-pair is expected to have a longer τ_0 (P/N = 0, <1 ms; P/N = 0.3, 29 ms; P/N = 0.9, 106 ms) and a larger K_{op} (P/N = 0, 0.76×10^{-6}; P/N = 0.3, 0.95×10^{-6}; P/N = 0.9, 1.31×10^{-6}), as the protein/DNA (P/N) molar ratio increases (Fig. 2C) [49].

In addition, if k_{cl} ($= k_{op}/K_{op}$) is much larger than $k_B[B]$, Eq. (5) simplifies to:

$$k_{ex} = K_{op}k_B[B] \quad (7)$$

In this case, the K_{op} values can be determined from the slope of the linear correlation between the k_{ex} and [B] (Fig. 2D) [28]. The imino proton of a less stable base-pair with larger K_{op} has a larger slope in these plots. For example, in the (-1C)-mutant P1 duplex of *Tetrahymena* ribozyme, the U20·A3 base-pair is expected to be less stable with a larger K_{op} than the A24·U-3 and G23·C-2 base-pairs (K_{op} of U20·A3, 83×10^{-6}; A24·U-3, 21×10^{-6}; G23·C-2, $<1.5 \times 10^{-6}$) (Fig. 2D) [28].

The Gibbs free energy difference (ΔG^o_{bp}) between the closed and open states is calculated from the equilibrium constant for base-pair opening using Eq. (8):

$$\Delta G^o_{bp} = -\Delta G^o_{opening} = RT\ \ln(K_{op}) \quad (8)$$

where $\Delta G^o_{opening}$ is the Gibbs free energy change in the opening process, T is the absolute temperature and R is the universal gas constant [20,21,31]. The activation energies for base-pair opening ($\Delta G^{\ddagger}_{op}$) and closing ($\Delta G^{\ddagger}_{cl}$) are related to the k_{op} and k_{cl} values, respectively, by the Arrhenius equation. The differences in ΔG^o_{bp} and activation energies for base-pair opening ($\Delta\Delta G^{\ddagger}_{op}$) and closing ($\Delta\Delta G^{\ddagger}_{cl}$) in wild-type and modified nucleic acids are calculated using Eqs. (9), (10), and (11), respectively:

$$\Delta\Delta G^o_{bp} = \Delta G^o_{bp,\,mod} - \Delta G^o_{bp,wt} = RT\ \ln(K_{op,\,mod}/K_{op,wt}) \quad (9)$$

$$\Delta\Delta G^{\ddagger}_{op} = \Delta G^{\ddagger}_{op,\,mod} - \Delta G^{\ddagger}_{op,wt} = -RT\ \ln(k_{op,\,mod}/k_{op,wt}) = RT\ \ln(\tau_{op,\,mod}/\tau_{op,wt}) \quad (10)$$

$$\Delta\Delta G^{\ddagger}_{cl} = \Delta G^{\ddagger}_{cl,\,mod} - \Delta G^{\ddagger}_{cl,wt} = -RT\ \ln(k_{cl,\,mod}/k_{cl,wt}) = RT\ \ln(\tau_{open,\,mod}/\tau_{open,wt}) \quad (11)$$

where the subscripts, wt and mod, indicate the thermodynamic parameters of the wild-type and modified nucleic acids, respectively [20,31].

2.2. NMR Measurement of Hydrogen Exchange Rates

The hydrogen exchange rates of the imino protons were determined by a water magnetization transfer experiment, where a selective 180° pulse for water was applied, followed by a variable delay (t), and then a Watergate acquisition pulse was used to suppress the water signal [27,28,52]. During the delay times between selective water inversion and acquisition pulses, a weak gradient (0.02 G/cm) was applied to prevent the radiation damping of the water signal [27,28]. The exchange rate constants (k_{ex}) were determined by fitting the relative peak intensities, $I(t)/I_0$, of the imino protons to:

$$\frac{I(t)}{I_0} = 1 - 2\frac{k_{ex}}{(R_{1w} - R_{1a})}\left(e^{-R_{1a}t} - e^{-R_{1w}t}\right) \quad (12)$$

where $I(t)$ and I_0 are the peak intensities of the imino proton at delay times t and zero, respectively, R_{1a} and R_{1w} are the apparent relaxation rate constants for the imino protons and water, respectively, which were determined by inversion recovery experiments [28].

The water magnetization transfer method is prone to some artifacts such as exchange-relayed NOE from rapidly exchanging protons in nucleic acids [53]. To suppress efficiently this artifact, a phase-modulated CLEAN chemical exchange spectroscopy (CLEANEX-PM) was applied to the mixing period of a water-selective pulse sequence [53]. The hydrogen exchange data for various nucleic acids using CLEANEX-PM have been reported [53–56].

Generally, the imino protons in double-helical regions have relatively fast exchange kinetics (k_{ex} = 0.1–100 s^{-1} at 25 °C). Interestingly, very slowly exchanging imino protons have been observed for modified tRNAs [57–59]. Hydrogen-deuterium exchange experiments were used to probe the dynamics and flexibility of the slowly exchanging imino protons in various nucleic acid systems [57–62].

3. Implications for Specific DNA Recognition

3.1. Recognition of Hemimethylated GATC Site

Many DNA binding proteins recognize their particular DNA sequences in a highly selective manner. The DNA-protein interactions require sequence-specific hydrogen bonding, van der Waals interactions, sequence-dependent structural changes. In addition, the flexibility of a DNA duplex to adopt the unique structure in complex is important in sequence-specific recognition. Enzymatic methylation of DNA occurs abundantly in most living organisms and regulates a variety of cellular processes. *Escherichia coli* (*E. coli*) DNA adenine methyltransferase (dam) methylates the N6 of adenines, to form the N6-methylated A (m^6A), within 5'-GATC-3′ sites at the replication origin *oriC* [63]. The *E. coli* seqA protein prefers to bind to newly synthesized, hemimethylated, rather than fully methylated, GATC sites to inhibit the initiation of the second round of chromosomal replication [64]. It was reported that the m^6A modification destabilizes the base-pairing of RNA duplexes, because the m^6A exhibited high energy *anti* conformation to maintain the Watson-Crick m^6A·T base-pair [65–67]. However, in the GATC-containing DNA duplexes, the m^6A methylation at the GATC site stabilized the base-pairs at the GATC site [20]. The crystal structure of the seqA protein complexed with a hemimethylated GATC sequence revealed that the two G·C base-pairs exhibited longer heavy atom distances between G-O6 and C-N4 than that of a Watson-Crick base-pair (*see* Fig. 1), indicating the a partially opened G·C base-pair [68]. However, in the solution structure of the DNA duplex containing hemimethylated GATC, these two base-pairs formed the stable Watson-Crick base-pairs [69]. Interestingly, NMR hydrogen exchange studies revealed that the $\Delta\Delta G^{\ddagger}_{cl}$ value, calculated using Eq. (11), of the 3′-neighboring

G·C base-pair of the N6-methylated adenine between the DNA duplexes containing the hemimthylated and fully methylated GATC sites is 1.42 kcal/mol, although the $\Delta\Delta G^{o}_{bp}$ value, calculated using Eq. (9), is only 0.17 kcal/mol (Fig. 3A) [20]. Using free energy differences calculated from these hydrogen exchange data as shown in Fig. 3A, it was shown that the partial opening of the G·C base pairs in the hemimethylated GATC sequence required a much smaller amount of energy than fully methylated GATC (Fig. 3A) [20]. Thus, it was concluded that the hemimethylated GATC site is energetically more favorable for complex formation with seqA than the corresponding fully methylated complex [20].

3.2. Recognition of Cyclobutane Pyrimidine Dimer

The CPD is one of the major types of cytotoxic, mutagenic and carcinogenic UV-induced DNA photoproducts [70,71]. In mammalian cells, CPD-damaged DNA is repaired by nucleotide excision repair [71,72], which is initiated by the binding of XPC-hHR23B to the site of DNA damage [73,74]. Although the CPD lesions are recognized poorly by XPC-hHR23B, when CPD lesions have double T·G mismatches, the binding affinity of XPC-hHR23B is dramatically increased [74]. A structural study of CPD-containing DNA duplexes suggested that, during nucleotide excision repair, the XPC-hHR23B complex recognizes DNA damage by directly searching for conformational distortions, such as a flexible backbone, a bent helix, or an unusual groove width [75]. NMR hydrogen exchange studies found that the two thymine bases of a CPD formed stable Watson-Crick base-pairs with the two opposite adenine bases, evident by a $\Delta\Delta G^{o}_{bp}$ ~ 0.2 kcal/mol relative to normal Watson-Crick T·A base-pairs [21]. When the CPD forms double T·G base-pairs, the $\Delta\Delta G^{o}_{bp}$ values are >1.9 kcal/mol [21]. Interestingly, these base-pair instabilities extended to the two base-pair neighbors, which had $\Delta\Delta G^{o}_{bp}$ values >1.4 kcal/mol [21]. Thus, this study concluded that a double mismatch at the CPD lesion facilitates the opening of the six base-pairs including the CPD, forming a small bubble structure that can be easily recognized by XPC-hHR23B [21].

4. Implications for Sequence-Specific RNA Cleavage

4.1. Biogenesis of miRNA156a

MicroRNAs (miRNAs) are small non-coding RNAs that negatively regulate expression of their target genes [76]. In plants, primary miRNAs are sequentially cleaved by DCL1 to make mature miRNA. MiRNA156 plays an important role in the temperature-responsive flowering of plants [77,78]. Plants overexpressing miRNA156 produced more leaves than wild-type plants before flowering by regulating the expression of the *SQUAMOSA promoter binding protein-like* (*SPL*) gene family [79,80]. The point mutations which stabilize the B5 bulge of primary miRNA156a affected the mature 156 levels as well as the leaf numbers at flowering of miRNA156 overexpressing plants [31,32]. NMR hydrogen exchange studies revealed that the C·G and U·A base-pairs at the DCL1 cleavage site exhibited unique base-pair stability and opening dynamics, which correlated with the biogenesis of miRNA156a [31,32]. For example, the C15·G98 base-pair in the A9C mutant, which decreased mature miRNA156 levels but decreased the leaf number at flowering compared to wild-type primary miRNA156a, was more stable with a $\Delta\Delta G^{o}_{bp}$ of −0.57 kcal/mol, and showed more dynamic opening/closing, with a $\Delta\Delta G^{\ddagger}_{cl}$ of −0.94 kcal/mol (Fig. 3B) [31]. Similar results were observed for the U16·A97 base-pair [31]. However, the A10G mutant, in which the C15·G98 base-pair had a $\Delta\Delta G^{o}_{bp}$ of 0.04 kcal/mol and a $\Delta\Delta G^{\ddagger}_{cl}$ of 0.30 kcal/mol (Fig. 3B), did not affect the mature miRNA156 levels or the flowering time of the plants [31]. Thus, it was concluded that precisely tuned base-pair stability/flexibility at the DCL1 cleavage

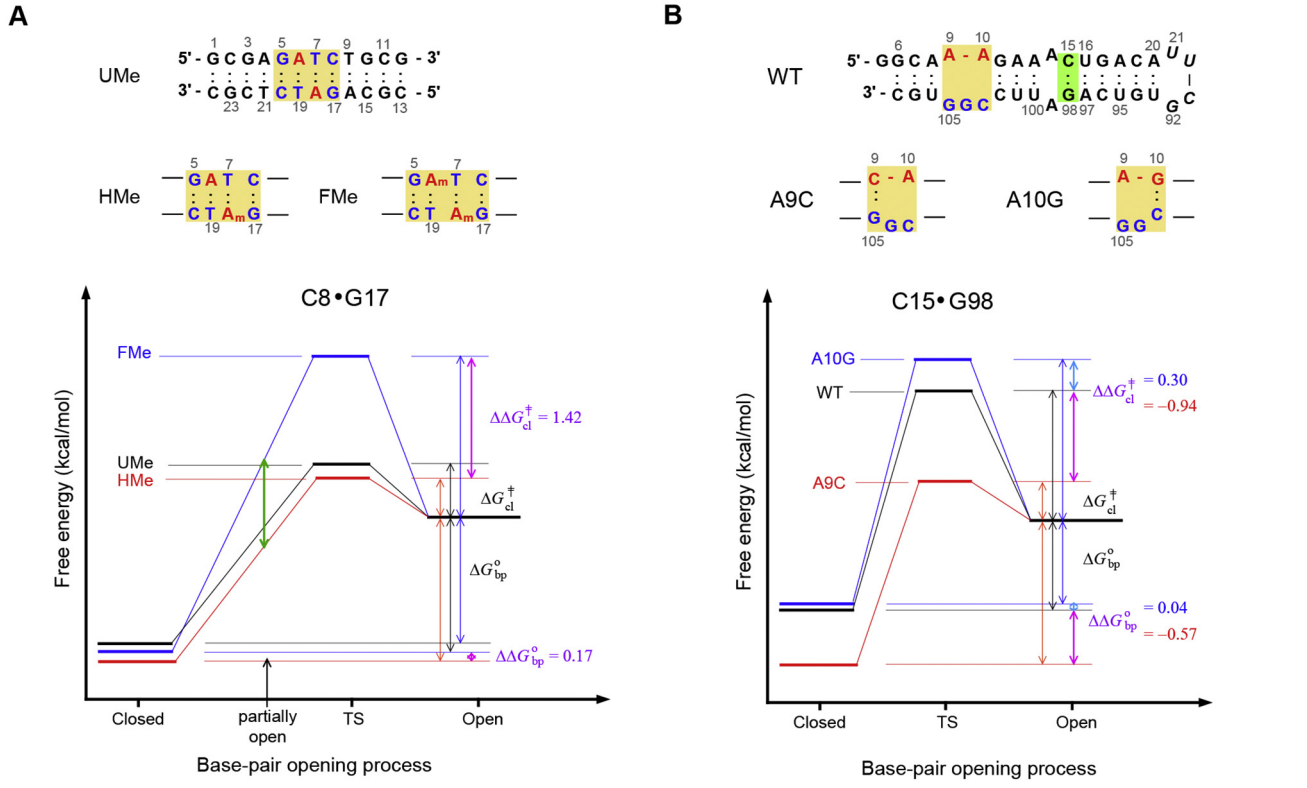

Fig. 3. Schematic representations of the Gibbs free energy diagram of the base-pair opening and closing for (A) the G·C base-pair adjacent to the N6-methylated adenine (A_m) residue in DNA duplexes containing unmethylated (UMe, black), hemimethylated (HMe, red), or fully methylated (FMe, blue) GATC sites [20] and (B) the C15·G98 base-pair in the WT (black), A9C (red) and A10G (blue) primary miRNA156a [33]. Secondary structures of the UMe-, HMe-, and FMe-GATC DNA in (A) and the WT, A9C, and A10G pri-miR156a in (B) are shown on top of each figure.

site is essential for efficient processing of primary miRNA156 and can be modulated by mutations adjacent to the cleavage site [31].

4.2. Self-Cleavage of the P1 Duplex of the Tetrahymena Group I Ribozyme

The *Tetrahymena* L-21 *Sca*I ribozyme is derived from the self-splicing group I intron and catalyzes a transesterification reaction in the P1 duplex formed with the internal guide sequence in the ribozyme and substrate RNA [81]. Various modifications of the P1 duplex have been shown to affect the cleavage reaction and kinetics for docking of the P1 duplex into the catalytic core [82,83]. NMR hydrogen exchange studies showed that the conserved U-1·G22 wobble pair, which is required for activity of the ribozyme (the cleavage site is the phosphodiester bond between A2 and U-1), destabilizes the neighboring A2·U21 base-pair, whereas the other neighboring C-2·G23 base-pair is the most stable base-pair in the P1duplex [28]. For efficient cleavage of substrate RNA, this P1 duplex docks into the catalytic core of the ribozyme and forms the active conformation [84,85]. In the active conformation, the G22 forms a tertiary interaction with adenine in the catalytic core and then the U-1·G22 wobble pair becomes destabilized [84,85]. Replacing the conserved U-1·G22 wobble pair with a Watson-Crick C·G base-pair leads to 200- and 9-fold smaller K_{op} values for this and the A2·U21 base-pairs, respectively, at the cleavage site [28]. This stabilization of the cleavage site explains the 80-fold increase of the undocking rate with the mutant sequence [83].

5. Implications for DNA/RNA-Protein Interactions

5.1. B-Z Transition of DNA by Z-DNA Binding Proteins

ZBPs play important roles in RNA editing, innate immune response and viral infection [86–88]. The crystal structures of ZBPs in complex with a 6-base-pair DNA duplex revealed that two molecules of ZBPs bind to each strand of double-stranded *Z*-DNA, yielding 2-fold symmetry with respect to the DNA helical axis [89–92]. ADAR1 deaminates adenine in pre-mRNA to yield inosine [89]. ADAR1 has two ZBPs, Zα and Zβ, at its NH2-terminus [89]. Hydrogen exchange measurements on the duplex DNA complexed with Zα domain of human ADAR1 ($Z\alpha_{ADAR1}$) revealed that the k_{ex} of the G imino protons in the left-handed Z-form helix decreased from 11.1 to 4.8 s^{-1} as the protein-to-DNA (P/N) molar ratio increased from 0.7 to 2.5 [50]. This observation indicates the possible presence of a mixture of two complex state: DNA-$Z\alpha_{ADAR1}$ and DNA-$(Z\alpha_{ADAR1})_2$ [50]. These results support an active B-Z transition mechanism in which the $Z\alpha_{ADAR1}$ protein first binds to B-DNA and then converts it to left-handed Z-DNA, a conformation that is then stabilized by the additional binding of a second $Z\alpha_{ADAR1}$ molecule [50]. Similar hydrogen exchange studies were performed for DNA duplexes complexed with other ZBPs [93–96].

5.2. B-Z Junction Formation in DNA by Z-DNA Binding Proteins

In order for ZBPs to produce Z-DNA in a section of long genomic DNA, two B-Z junctions must be formed at each end of the Z-DNA segment. A crystal structural study of a DNA duplex complexed with $Z\alpha_{ADAR1}$ showed that bases between B- and Z-DNA are almost continuously stacked, with the extrusion of one base-pair at the B-Z junction [97]. Hydrogen exchange studies of the DNA-$Z\alpha_{ADAR1}$ complexes showed that the k_{ex} values of the A·T base-pairs in AT-rich regions increased as the P/N ratio increased, indicating that $Z\alpha_{ADAR1}$ significantly destabilizes AT-rich regions [49,98]. However, $Z\alpha_{ADAR1}$ had little effect on the k_{ex} values of the G·C base-pairs in CG-rich regions [49,98]. In addition, the base-pair opening kinetics indicated that, in the complex, all G·C base-pairs have larger K_{op} values (smaller slopes in Fig. 2C) and longer τ_0 values (larger y-intercepts in Fig. 2C) than those of free DNA [49]. Thus, it was proposed that an intermediate structure exists during B-Z junction formation by $Z\alpha_{ADAR1}$, in which the DNA duplex displays unique dynamic features: (i) instability of the AT-rich region and (ii) a longer lifetime for the open state of the CG-rich region [49].

5.3. Target Recognition of RNA Aptamer

Macugen is the first modified RNA aptamer to be employed as a human therapeutic and was derived from an in vitro selection against the key angiogenic regulator protein, vascular endothelial growth factor, VEGF165 [99]. VEGF consists of two independent domains, a receptor-binding domain and a 55-amino acid heparin-binding domain (HBD) [100]. A photo-crosslinking study indicated that Macugen specifically recognizes VEGF by targeting the HBD [101]. NMR studies showed very similar secondary structure for Macugen, whether it is bound to the HBD or to VEGF165 [102]. These studies also found that the aptamer is stabilized by complex formation with either the HBD or VEGF165 [102]. Hydrogen exchange studies showed that many imino protons in the internal loop and neighboring base-pairs exhibit fast exchange in the free aptamer with very large k_{ex} values [51]. However, the k_{ex} values for many of these imino protons became much smaller upon binding of the HBD or VEGF165 [51]. These hydrogen exchange data support an induced-fit type mechanism in which RNAs with dynamic features in the free state can bind their target protein with extremely high affinity [51].

6. Implications for DNA-PNA Hybrid Duplex Formation

PNAs are one of the most widely used synthetic DNA mimics where the four bases are attached to a N-(2-aminoethyl)glycine (aeg) backbone [103,104]. Chimeric PNA (chiPNA), in which a chiral glycerol nucleic acid-like γ^3T monomer is incorporated into the aegPNA backbone, displays excellent RNA selectivity as well as antiparallel selectivity toward non-chimeric PNA [105]. Hydrogen exchange studies revealed that a aegPNA:DNA hybrid is a much more stable duplex (smaller K_{op}) and is less dynamic compared to the corresponding DNA duplex (longer τ_0 and τ_{open}) [38]. The γ^3T residue in the chiPNA:DNA hybrid destabilizes a specific base-pair (much larger k_{ex}) and its neighbors (3- to 60-fold larger K_{op}) compared to the non-chimeric PNA:DNA hybrid, while maintaining the thermal stabilities and dynamic properties of other base pairs [38]. In addition, the two neighboring base-pairs becomes more dynamic than in either the non-chimeric PNA:DNA hybrid or the corresponding DNA duplex (much shorter τ_0 and τ_{open}), meaning that these base-pairs open and reclose much more rapidly [38].

7. Conclusion

Base-pair opening in nucleic acids is a conformational transition that is required for their biological function. Hydrogen exchange is one of the widely used methods to study the thermodynamics and kinetics of base-pair opening in nucleic acids. The hydrogen exchange data of imino protons are analyzed based on a two-state (open/closed) model, where exchange only occurs from the open state. In this review, we discussed several examples of how hydrogen exchange data provide insight into the functional interactions of nucleic acids: 1) selective recognition of DNA by its target proteins; 2) regulation of RNA cleavage by site-specific mutations; 3) intermolecular interaction of proteins with their target DNA or RNA; 4) formation of PNA:DNA hybrid duplexes.

Declarations of Competing Interest

None.

Acknowledgements

This work was supported by the National Research Foundation of Korea [2017R1A2B2A001832], the Samsung Science and Technology Foundation [SSRF-BA1701-10], and the KBSI grant [D39700]. We

thank M. Stauffer, of Scientific Editing Solutions, for editing the manuscript.

References

[1] Leroy JL, Bolo N, Figueroa N, Plateau P, Guéron M. Internal motions of transfer RNA: a study of exchanging protons by magnetic resonance. J Biomol Struct Dyn 1985;2:915–39.
[2] Guéron M, Leroy JL. Studies of base pair kinetics by NMR measurement of proton exchange. Methods Enzymol 1995;261:383–413.
[3] Leijon M, Leroy JL. Internal motions of nucleic acid structures and the determination of base-pair lifetimes. Biochimie 1997;79:775–9.
[4] Moe JG, Russu IM. Proton exchange and base-pair opening kinetics in 5′-d(CGCGAATTCGCG)-3′ and related dodecamers. Nucleic Acids Res 1990;18:817–21.
[5] Leijon M, Gräslund A. Effects of sequence and length on imino proton exchange and base pair opening kinetics in DNA oligonucleotide duplexes. Nucleic Acids Res 1992;20:5339–43.
[6] Moe JG, Russu IM. Kinetics and energetics of base-pair opening in 5′-d(CGCGAATTCGCG)-3′ and a substituted dodecamer containing G·T mismatches. Biochemistry 1992;31:8421–8.
[7] Leijon M, Zdunek J, Fritzsche H, Sklenar H, Gräslund A. NMR studies and restrained-molecular-dynamics calculations of a long a+T-rich stretch in DNA. Effects of phosphate charge and solvent approximations. Eur J Biochem 1995;234:832–42.
[8] Folta-Stogniew E, Russu IM. Base-catalysis of imino proton exchange in DNA: effects of catalyst upon DNA structure and dynamics. Biochemistry 1996;35:8439–49.
[9] Nonin S, Jiang F, Patel DJ. Imino proton exchange and base pair kinetics in the AMP-RNA aptamer complex. J Mol Biol 1997;268:359–74.
[10] Dornberger U, Leijon M, Fritzsche H. High base pair opening rates in tracts of GC base pairs. J Biol Chem 1999;274:6957–62.
[11] Wärmländer S, Sen A, Leijon M. Imino proton exchange in DNA catalyzed by ammonia and trimethylamine: evidence for a secondary long-lived open state of the base pair. Biochemistry 2000;39:607–15.
[12] Snoussi K, Leroy JL. Alteration of a·T base-pair opening kinetics by the ammonium cation in DNA A-tracts. Biochemistry 2002;41:12467–74.
[13] Bhattacharya PK, Cha J, Barton JK. ^{1}H NMR determination of base-pair lifetimes in oligonucleotides containing single base mismatches. Nucleic Acids Res 2002;30:4740–50.
[14] Wärmländer S, Sandström K, Leijon M, Gräslund A. Base-pair dynamics in an antiparallel DNA triplex measured by catalyzed imino proton exchange monitored via ^{1}H NMR spectroscopy. Biochemistry 2003;42:12589–95.
[15] Várnai P, Canalia M, Leroy JL. Opening mechanism of G·T/U pairs in DNA and RNA duplexes: a combined study of imino proton exchange and molecular dynamics simulation. J Am Chem Soc 2004;126:14659–67.
[16] Coman D, Russu IM. A nuclear magnetic resonance investigation of the energetics of basepair opening pathways in DNA. Biophys J 2005;89:3285–92.
[17] Every AE, Russu IM. Influence of magnesium ions on spontaneous opening of DNA base pairs. J Phys Chem B 2008;112:7689–95.
[18] Cho SJ, Bang J, Lee JH, Choi BS. Base pair opening kinetics and dynamics in the DNA duplexes that specifically recognized by very short patch repair protein (Vsr). Arch Biochem Biophys 2010;501:201–6.
[19] Parker JB, Stivers JT. Dynamics of uracil and 5-fluorouracil in DNA. Biochemistry 2011;50:612–7.
[20] Bang J, Bae SH, Park CJ, Lee JH, Choi BS. Structural and dynamics study of DNA dodecamer duplexes that contain un-, hemi- or fully-methylated GATC sites. J Am Chem Soc 2008;130:17688–96.
[21] Szulik MW, Voehler MW, Ganguly M, Gold B, Stone MP. Site-specific stabilization of DNA by a tethered major groove amine, 7-aminomethyl-7-deaza-2′-deoxyguanosine. Biochemistry 2013;52:7659–68.
[22] Bang J, Kang YM, Park CJ, Lee JH, Choi BS. Thermodynamics and kinetics for base pair opening in the decamer DNA duplexes containing cyclobutane pyrimidine dimer. FEBS Lett 2009;583:2037–41.
[23] Dhavan GM, Lapham J, Yang S, Crothers DM. Decreased imino proton exchange and base-pair opening in the IHF-DNA complex measured by NMR. J Mol Biol 1999;288:659–71.
[24] Friedman JI, Jiang YL, Stivers JT. Unique dynamic properties of DNA duplexes containing interstrand cross-links. Biochemistry 2011;50:882–90.
[25] Esmaili N, Leroy JL. I-motif solution structure and dynamics of the d(AACCCC) and d(CCCCAA) tetrahymena telomeric repeats. Nucleic Acids Res 2005;33:213–24.
[26] Canalia M, Leroy JL. Structure, internal motions and association-dissociation kinetics of the i-motif dimer of d(5mCCTCACTCC). Nucleic Acids Res 2005;33:5471–81.
[27] Snoussi K, Leroy JL. Imino proton exchange and base-pair kinetics in RNA duplexes. Biochemistry 2001;40:8898–904.
[28] Lee JH, Pardi A. Thermodynamics and kinetics for base pair opening in the P1 duplex of *Tetrahymena* group I ribozyme. Nucleic Acids Res 2007;35:2965–74.
[29] Hao ZX, Tan M, Liu CD, Feng R, Wang ED, Zhu G. Studying base pair open-close kinetics of tRNA^{Leu} by TROSY-based proton exchange NMR spectroscopy. FEBS Lett 2010;584:4449–52.
[30] Chen C, Jiang L, Michalczyk R, Russu IM. Structural energetics and base-pair opening dynamics in sarcin-ricin domain RNA. Biochemistry 2006;45:13606–13.
[31] Kim W, Kim HE, Lee AR, Jun AR, Jung MG, Ahn JH, et al. Base-pair opening dynamics of primary miR156a using NMR elucidates structural determinants important for its processing level and leaf number phenotype in *Arabidopsis*. Nucleic Acids Res 2017;45:875–85.
[32] Kim HE, Kim W, Lee AR, Jin S, Jun AR, Kim NK, et al. Base-pair opening dynamics of the microRNA precursor pri-miR156a affect temperature-responsive flowering in *Arabidopsis*. Biochem Biophys Res Commun 2017;484:839–44.
[33] Rinnenthal J, Klinkert B, Narberhaus F, Schwalbe H. Direct observation of the temperature-induced melting process of the Salmonella fourU RNA thermometer at base-pair resolution. Nucleic Acids Res 2010;38:3834–47.
[34] Wagner D, Rinnenthal J, Narberhaus F, Schwalbe H. Mechanistic insights into temperature-dependent regulation of the simple cyanobacterial hsp17 RNA thermometer at base-pair resolution. Nucleic Acids Res 2015;43:5572–85.
[35] Mirau PA, Kearns DR. Effect of environment, conformation, sequence and base substituents on the imino proton exchange rates in guanine and inosine-containing DNA, RNA, and DNA-RNA duplexes. J Mol Biol 1984;177:207–27.
[36] Steinert HS, Rinnenthal J, Schwalbe H. Individual basepair stability of DNA and RNA studied by NMR-detected solvent exchange. Biophys J 2012;102:2564–74.
[37] Leijon M, Sehlstedt U, Nielsen PE, Gräslund A. Unique base-pair breathing dynamics in PNA-DNA hybrids. J Mol Biol 1997;271:438–55.
[38] Seo YJ, Lim J, Lee EH, Ok T, Yoon J, Lee JH, et al. Base-pair opening kinetics study of the *aeg*PNA:DNA hydrid duplex containing a site-specific GNA-like chiral PNA monomer. Nucleic Acids Res 2011;39:7329–35.
[39] Anosova I, Kowal EA, Sisco NJ, Sau S, Liao JY, Bala S, et al. Structural insights into conformation differences between DNA/TNA and RNA/TNA chimeric duplexes. ChemBioChem 2016;17:1705–8.
[40] Legault P, Pardi A. Unusual dynamics and pK_a shift at the active site of a lead-dependent ribozyme. J Am Chem Soc 1997;119:6621–8.
[41] Ravindranathan S, Butcher SE, Feigon J. Adenine protonation in domain B of the hairpin ribozyme. Biochemistry 2000;39:16026–32.
[42] Reiter NJ, Blad H, Abildgaard F, Butcher SE. Dynamics in the U6 RNA intramolecular stem-loop: a base flipping conformational change. Biochemistry 2004;43:13739–47.
[43] Shrestha P, Cui Y, Wei J, Jonchhe S, Mao H. Single-molecule mechanochemical pH sensing revealing the proximity effect of hydroniums generated by an alkaline phosphatase. Anal Chem 2018;90:1718–24.
[44] Yang L, Zhong Z, Tong C, Jia H, Liu Y, Chen G. Single-molecule mechanical folding and unfolding of RNA hairpins: effects of single A-U to a·C pair substitutions and single proton binding and implications for mRNA structure-induced −1 ribosomal frameshifting. J Am Chem Soc 2018;140:8172–84.
[45] Cao C, Jiang YL, Stivers JT, Song F. Dynamic opening of DNA during the enzymatic search for a damaged base. Nat Struct Mol Biol 2004;11:1230–6.
[46] Cao C, Jiang YL, Krosky DJ, Stivers JT. The catalytic power of uracil DNA glycosylase in the opening of thymine base pairs. J Am Chem Soc 2006;128:13034–5.
[47] Parker JB, Bianchet MA, Krosky DJ, Friedman JI, Amzel LM, Stivers JT. Enzymatic capture of an extrahelical thymine in the search for uracil in DNA. Nature 2007;449:433–7.
[48] Friedman JI, Majumdar A, Stivers JT. Nontarget DNA binding shapes the dynamic landscape for enzymatic recognition of DNA damage. Nucleic Acids Res 2009;37:3493–500.
[49] Lee YM, Kim HE, Park CJ, Lee AR, Ahn HC, Cho SJ, et al. NMR study on the B-Z junction formation of DNA duplexes induced by Z-DNA binding domain of human ADAR1. J Am Chem Soc 2012;134:5276–83.
[50] Kang YM, Bang J, Lee EH, Ahn HC, Seo YJ, Kim KK, et al. NMR spectroscopic elucidation of the B-Z transition of a DNA double helix induced by the Zα domain of the human ADAR1. J Am Chem Soc 2009;131:11485–91.
[51] Lee JH, Jucker F, Pardi A. Imino proton exchange rates imply an induced-fit binding mechanism for the VEGF$_{165}$-targeted aptamer, Macugen. FEBS Lett 2008;582:1835–9.
[52] Liu M, Mao X, Ye C, Huang H, Nicholson JK, Lindon JC. Improved WATERGATE pulse sequences for solvent suppression in NMR spectroscopy. J Magn Reson 1998;132:125–9.
[53] Hwang TL, Mori S, Shaka AJ, van Zijl PCM. Application of phase-modulated CLEAN chemical EXchange spectroscopy (CLEANEX-PM) to detect water−protein proton exchange and intermolecular NOEs. J Am Chem Soc 1997;119:6203–4.
[54] Rennella E, Sára T, Juen M, Wunderlich C, Imbert L, Solyom Z, et al. RNA binding and chaperone activity of the *E. coli* cold-shock protein CspA. Nucleic Acids Res 2017;45:4255–68.
[55] Strebitzer E, Rangadurai A, Plangger R, Kremser J, Juen MA, Tollinger M, et al. 5-Oxyacetic acid modification destabilizes double helical stem structures and favors anionic Watson-crick like cmo^{5}U-G base pairs. Chem A Eur J 2018;24:18903–6.
[56] Lee YM, Lee EH, Seo YJ, Kang YM, Ha JH, Kim HE, et al. Measurement of hydrogen exchange times of the RNA imino protons using by phase-modulated CLEAN chemical exchange spectroscopy. Bull Korean Chem Soc 2009;30:2197–8.
[57] Johnston PD, Figueroa N, Redfield AG. Real-time solvent exchange studies of the imino and amino protons of yeast phenylalanine transfer RNA by Fourier transform NMR. Proc Natl Acad Sci U S A 1979;76:3130–4.
[58] Figueroa N, Keith G, Leroy JL, Plateau P, Roy S, Guéron M. NMR study of slowly exchanging imino protons in yeast tRNA^{asp}. Proc Natl Acad Sci U S A 1983;80:4330–3.
[59] Vermeulen A, McCallum SA, Pardi A. Comparison of the global structure and dynamics of native and unmodified tRNA^{val}. Biochemistry 2005;44:6024–33.
[60] Cheong C, Moore PB. Solution structure of an unusually stable RNA tetraplex containing G- and U-quartet structures. Biochemistry 1992;31:8406–14.
[61] Nozinovic S, Fürtig B, Jonker HR, Richter C, Schwalbe H. High-resolution NMR structure of an RNA model system: the 14-mer cUUCGg tetraloop hairpin RNA. Nucleic Acids Res 2010;38:683–94.
[62] Lee JH. Hydrogen-deuterium exchange of *Tetrahymena* group I ribozyme. Bull Korean Chem Soc 2007;28:1643–4.
[63] Geier GE, Modrich P. Recognition sequence of the dam methylase of *Escherichia coli* K12 and mode of cleavage of Dpn I endonuclease. J Biol Chem 1979;254:1408–13.

[64] Lu M, Campbell JL, Boye E, Kleckner N. SeqA: a negative modulator of replication initiation in *E. coli*. Cell 1994;77:413–26.
[65] Engel JD, von Hippel PH. Effects of methylation on the stability of nucleic acid conformations: studies at the monomer level. Biochemistry 1974;13:4143–58.
[66] Micura R, Pils W, Höbartner C, Grubmayr K, Ebert MO, Jaun B. Methylation of the nucleobases in RNA oligonucleotides mediates duplex-hairpin conversion. Nucleic Acids Res 2001;29:3997–4005.
[67] Roost C, Lynch SR, Batista PJ, Qu K, Chang HY, Kool ET. Structure and thermodynamics of N6-methyladenosine in RNA: a spring-loaded base modification. J Am Chem Soc 2015;137:2107–15.
[68] Guarne A, Zhao Q, Ghirlando R, Yang W. Insights into negative modulation of *E. coli* replication initiation from the structure of SeqA-hemimethylated DNA complex. Nat Struct Biol 2002;9:839–43.
[69] Bae SH, Cheong HK, Cheong C, Kang S, Hwang DS, Choi BS. Structure and dynamics of hemimethylated GATC sites: implications for DNA-SeqA recognition. J Biol Chem 2003;278:45987–93.
[70] Mitchell DL. (1988) the relative cytotoxicity of (6-4) photoproducts and cyclobutane dimers in mammalian cells. Photochem Photobiol 1988;48:51–7.
[71] Park CJ, Lee JH, Choi BS. Functional insights gained from structural analyses of DNA duplexes that contain UV-damaged photoproducts. Photochem Photobiol 2007;83:187–95.
[72] de Laat WL, Jaspers NG, Hoeijmakers JH. Molecular mechanism of nucleotide excision repair. Genes Dev 1999;13:768–85.
[73] Sugasawa K, Ng JM, Masutani C, Iwai S, van der Spek PJ, Eker AP, et al. Xeroderma pigmentosum group C protein complex is the initiator of global genome nucleotide excision repair. Mol Cell 1988;2:223–32.
[74] Sugasawa K, Okamoto T, Shimizu Y, Masutani C, Iwai S, Hanaoka F. A multistep damage recognition mechanism for global genomic nucleotide excision repair. Genes Dev 2001;15:507–21.
[75] Lee JH, Park CJ, Shin JS, Ikegami T, Akutsu H, Choi BS. NMR structure of the DNA decamer duplex containing double T·G mismatches of *cis-syn* cyclobutane pyrimidine dimer: implications for DNA damage recognition by the XPC-hHR23B complex. Nucleic Acids Res 2004;32:2474–81.
[76] Carrington JC, Ambros V. Role of microRNAs in plant and animal development. Science 2003;301:336–8.
[77] Zhou CM, Wang JW. Regulation of flowering time by microRNAs. J Genet Genomics 2013;40:211–5.
[78] Kim W, Ahn JH. MicroRNA-target interactions: important signaling modules regulating flowering time in diverse plant species. Crit Rev Plant Sci 2014;33:470–85.
[79] Kim JJ, Lee JH, Kim W, Jung HS, Huijser P, Ahn JH. The microRNA156-SQUAMOSA PROMOTER BINDING PROTEIN-LIKE3 module regulates ambient temperature-responsive flowering via FLOWERING LOCUS T in Arabidopsis. Plant Physiol 2012;159:461–78.
[80] Wu G, Poethig RS. Temporal regulation of shoot development in Arabidopsis thaliana by miR156 and its target SPL3. Development 2006;133:3539–47.
[81] Been MD, Cech TR. One binding-site determines sequence specificity of Tetrahymena pre-ribosomal-RNA self-splicing, transsplicing, and RNA enzyme-activity. Cell 1986;47:207–16.
[82] Karbstein K, Carroll KS, Herschlag D. (2002) probing the *Tetrahymena* group I ribozyme reaction in both directions. Biochemistry 2002;41:11171–83.
[83] Bartley LE, Zhuang X, Das R, Chu S, Herschlag D. Exploration of the transition state for tertiary structure formation between an RNA helix and a large structured RNA. J Mol Biol 2003;328:1011–26.
[84] Adams PL, Stahley MR, Kosek AB, Wang J, Strobel SA. Crystal structure of a self-splicing group I intron with both exons. Nature 2004;430:45–50.
[85] Golden BL, Kim H, Chase E. Crystal structure of a phage Twort group I ribozyme-product complex. Nat Struct Mol Biol 2005;12:82–9.
[86] Herbert A, Rich A. The biology of left-handed Z-DNA. J Biol Chem 1996;271:11595–8.
[87] Herbert A, Rich A. Left-handed Z-DNA: structure and function. Genetica 1999;106:37–47.
[88] Rich A, Zhang S. Z-DNA: the long road to biological function. Nat Rev Genet 2003;4:566–72.
[89] Schwartz T, Rould MA, Lowenhaupt K, Herbert A, Rich A. Crystal structure of the Zα domain of the human editing enzyme ADAR1 bound to left-handed Z-DNA. Science 1999;284:1841–5.
[90] Schwartz T, Behlke J, Lowenhaupt K, Heinemann U, Rich A. Structure of the DLM-1-Z-DNA complex reveals a conserved family of Z-DNA-binding proteins. Nat Struct Biol 2001;8:761–5.
[91] Ha SC, Lokanath NK, van Quyen D, Wu CA, Lowenhaupt K, Rich A, et al. A poxvirus protein forms a complex with left-handed Z-DNA: crystal structure of a Yatapoxvirus Zα bound to DNA. Proc Natl Acad Sci U S A 2004;101:14367–72.
[92] Kim D, Hur J, Park K, Bae S, Shin D, Ha SC, et al. Distinct Z-DNA binding mode of a PKR-like protein kinase containing a Z-DNA binding domain (PKZ). Nucleic Acids Res 2014;42:5937–48.
[93] Lee EH, Seo YJ, Ahn HC, Kang YM, Kim HE, Lee YM, et al. NMR study of hydrogen exchange during the B-Z transition of a DNA duplex induced by the Zα domain of yatapoxvirus E3L. FEBS Lett 2010;584:4453–7.
[94] Kim HE, Ahn HC, Lee YM, Lee EH, Seo YJ, Kim YG, et al. The Zβ domain of human DAI binds to Z-DNA via a novel B-Z transition pathway. FEBS Lett 2011;585:772–8.
[95] Seo YJ, Ahn HC, Lee EH, Bang J, Kang YM, Kim HE, et al. Sequence discrimination of the Zα domain of human ADAR1 during B-Z transition of DNA duplexes. FEBS Lett 2010;584:4344–50.
[96] Lee AR, Park CJ, Cheong HK, Ryu KS, Park JW, Kwon MY, et al. Solution structure of Z-DNA binding domain of PKR-like protein kinase from *Carassius auratus* and quantitative analyses of intermediate complex during B-Z transition. Nucleic Acids Res 2016;44:2936–48.
[97] Ha SC, Lowenhaupt K, Rich A, Kim YG, Kim KK. Crystal structure of a junction between B-DNA and Z-DNA reveals two extruded bases. Nature 2005;437:1183–6.
[98] Lee YM, Kim HE, Lee EH, Seo YJ, Lee AR, Lee JH. NMR investigation on the DNA binding mode and B-Z transition pathway of the Zα domain of human ADAR1. Biophys Chem 2013;172:18–25.
[99] Ng EW, Shima DT, Calias P, Cunningham Jr ET, Guyer DR, Adamis AP. Pegaptanib, a targeted anti-VEGF aptamer for ocular vascular disease. Nat Rev Drug Discov 2006;5:123–32.
[100] Ferrara N, Gerber HP, LeCouter J. The biology of VEGF and its receptors. Nat Med 2003;9:669–76.
[101] Ruckman J, Green LS, Beeson J, Waugh S, Gillette WL, Henninger DD, et al. 2'-Fluoropyrimidine RNA-based aptamers to the 165-amino acid form of vascular endothelial growth factor (VEGF165). J Biol Chem 1998;273:20556–67.
[102] Lee JH, Canny MD, de Erkenez A, Krilleke D, Ng YS, Shima DT, et al. A therapeutic aptamer inhibits angiogenesis by specifically targeting the heparin binding domain of VEGF165. Proc Natl Acad Sci U S A 2005;102:18902–7.
[103] Nielsen PE, Egholm M, Berg RH, Buchardt O. Sequence-selective recognition of DNA by strand displacement with a thymine-substituted polyamide. Science 1991;254:1497–500.
[104] Egholm M, Buchardt O, Nielsen PE. Peptide nucleic acids (PNA). Oligonucleotide analogs with an achiral peptide backbone. J Am Chem Soc 1992;114:1895–7.
[105] Ok T, Lee J, Jung C, Lim J, Park CM, Lee JH, et al. GNA/aegPNA chimera loaded with RNA binding preference. Chem Asian J 2011;6:1996–9.